Investigating the Global Performance of the BDS-2 and BDS-3 Joint Real-Time Undifferenced and Uncombined Precise Point Positioning Using RTS Products from Different Analysis Center...

Article *in* Remote Sensing · February 2024

DOI: 10.3390/rs16050788

CITATIONS
0

READS
31

7 authors, including:

Ahao Wang
China University of Mining and Technology-Beijing
24 PUBLICATIONS **217** CITATIONS
SEE PROFILE

Yize Zhang
Chinese Academy of Sciences
95 PUBLICATIONS **595** CITATIONS
SEE PROFILE

Junping Chen
Chinese Academy of Sciences
159 PUBLICATIONS **1,671** CITATIONS
SEE PROFILE

remote sensing

MDPI

Article

Investigating the Global Performance of the BDS-2 and BDS-3 Joint Real-Time Undifferenced and Uncombined Precise Point Positioning Using RTS Products from Different Analysis Centers

Ahao Wang [1], Yize Zhang [2,*], Junping Chen [2,3], Hu Wang [4], Tianning Luo [1], Mingyou Gong [1] and Quanpeng Liu [1]

[1] College of Geoscience and Surveying Engineering, China University of Mining and Technology-Beijing, Beijing 100083, China; ahao_wang@cumtb.edu.cn (A.W.); 2110200215@student.cumtb.edu.cn (T.L.); 2110200114@student.cumtb.edu.cn (M.G.); 2110200315@student.cumtb.edu.cn (Q.L.)
[2] Shanghai Astronomical Observatory, Chinese Academy of Sciences, Shanghai 200030, China; junping@shao.ac.cn
[3] School of Astronomy and Space Science, University of Chinese Academy of Sciences, Beijing 100049, China
[4] Chinese Academy of Surveying & Mapping, Beijing 100036, China; wanghu@casm.ac.cn
* Correspondence: zhyize@shao.ac.cn

Abstract: Compared to the traditional ionospheric-free (IF) precise point positioning (PPP) model, the undifferenced and uncombined (UU) PPP has the advantages of lower observation noise and the ability to obtain ionospheric information. Thanks to the IGS (International GNSS Service), real-time service (RTS) can provide RT vertical total electron content (VTEC) products, and an enhanced RT UU-PPP based on the RT-VTEC constraints can be achieved. The global performance of the BeiDou Navigation Satellite System-2 (BDS-2) and BDS-3 joint RT UU-PPP using different RTS products was investigated. There is not much difference in the RTS orbit accuracy of medium earth orbit (MEO) satellites among all analysis centers (ACs), and the optimal orbit accuracy is better than 5, 9, and 7 cm in the radial, along-track, and cross-track directions, respectively. The orbit accuracy of inclined geosynchronous orbit (IGSO) satellites is worse than that of MEO satellites. Except for CAS of 0.46 ns, the RTS clock accuracy of MEO satellites for other ACs achieves 0.2–0.27 ns, and the corresponding accuracy is about 0.4 ns for IGSO satellites. In static positioning, due to the limited accuracy of RT-VTEC, the convergence time of the enhanced RT UU-PPP is longer than that of RT IF-PPP for most ACs and can be better than 25 and 20 min in the horizontal and vertical components, respectively. After convergence, the 3D positioning accuracy of the static RT UU-PPP is improved by no more than 8.7%, and the optimal horizontal and vertical positioning accuracy reaches 3.5 and 7.0 cm, respectively. As for the kinematic mode with poor convergence performance, with the introduction of RT-VTEC constraints, the convergence time of RT UU-PPP can be slightly shorter and reaches about 55 and 60 min in the horizontal and vertical components, respectively. Both the horizontal and vertical positioning accuracies of the kinematic RT UU-PPP can be improved and achieve around 7.5 and 10 cm, respectively.

Keywords: BeiDou navigation satellite system (BDS); precise point positioning (PPP); real-time service (RTS); undifferenced and uncombined; convergence; positioning accuracy

Citation: Wang, A.; Zhang, Y.; Chen, J.; Wang, H.; Luo, T.; Gong, M.; Liu, Q. Investigating the Global Performance of the BDS-2 and BDS-3 Joint Real-Time Undifferenced and Uncombined Precise Point Positioning Using RTS Products from Different Analysis Centers. *Remote Sens.* **2024**, *16*, 788. https://doi.org/10.3390/rs16050788

Academic Editor: Baocheng Zhang

Received: 8 January 2024
Revised: 19 February 2024
Accepted: 22 February 2024
Published: 24 February 2024

1. Introduction

In the field of global navigation satellite system (GNSS) high-precision positioning, two representative technologies, real-time kinematic (RTK) and precise point positioning (PPP), have emerged successively. Due to the low cost and flexibility of using only one GNSS receiver, PPP technology has a wider range of applications than RTK and can be used for precise timing, atmospheric modeling, deformation monitoring, etc. [1–3]. The basis for the successful implementation of PPP is the adoption of precise satellite orbits and

clocks. In the early stage, the International GNSS Service (IGS) only provided final orbit and clock products with over ten days delay, as well as fast products with a delay of seventeen hours [4]. These products cannot meet the requirements of real-time (RT) PPP, which limits the application of PPP technology in fields such as earthquake and tsunami warnings, meteorological monitoring, and vehicle navigation. Since November 2010, ultra-rapid orbit and clock products have been provided by the IGS and can only support decimeter-level positioning accuracy due to the predicted clock accuracy of up to 3 ns [5,6]. In order to achieve real-time and centimeter-level PPP, the IGS started providing free real-time service (RTS) products in April 2013. These products are broadcasted through the internet in the form of state space representation (SSR) corrections [7]. Using IGS final products as a reference, the root mean square (RMS) of orbit errors and standard deviation (STD) of clock errors for GPS/Galileo satellites can be lower than 5 cm and 0.2 ns, respectively. The orbit accuracy of GLONASS satellites is relatively low at about 8 cm, and the clock accuracy may be sharply decreased to over 0.5 ns [8,9]. The validation of RT PPP shows that the RMS positioning accuracy using RTS products can be improved by around 50% compared to the solution using ultra-rapid products [6]. The horizontal positioning accuracy of the RT PPP using single system dual-frequency (DF) observations in kinematic mode has the ability to achieve 2–5 cm and the vertical component can be better than 10 cm [8].

Compared to other GNSSs, the BeiDou Navigation Satellite System (BDS) was developed and provided services relatively late. BDS-2 and BDS-3 started providing Asia–Pacific regional and global positioning, navigation, and timing (PNT) services in December 2012 and July 2020, respectively [10]. As for geostationary earth orbit (GEO) satellites of BDS-2, the RTS orbit accuracy can reach up to 2 m in the along-track and cross-track directions, and the radial errors only achieve decimeter-level accuracy [8]. The RTS orbit accuracy of BDS-2 inclined geosynchronous orbit (IGSO) and medium earth orbit (MEO) satellites is displayed at the centimeter level in the radial direction and 0.1–0.2 m in other directions. In terms of BDS-2 clock accuracy, the mean STD of GEO and IGSO/MEO satellites exceeds 1.0 and 0.5 ns, respectively. The quality of RTS orbits and clocks of BDS-3 satellites is generally better than that of BDS-2 satellites, especially for satellite clocks. The STD clock accuracy of BDS-3 satellites, except for IGSO satellites, can reach about 0.35 ns [8,11]. Currently, most research on the assessment of BDS RTS products is mainly focused on the early stages (i.e., 2020–2021) of BDS-3 full completion. With the hardware and software upgrades of the GNSS receivers, more and more IGS monitoring stations can be used to track BDS-3 satellites, and it is worth exploring whether the accuracy of BDS RTS products has been improved. In this contribution, a comprehensive assessment was conducted on both BDS-2 and BDS-3 RTS products for five analysis centers (ACs) at the end of 2022. This work is important for current BDS real-time users and has the potential to provide a critical guide for numerous engineering applications.

Due to the complexity and variability of ionospheric delay errors and the limited accuracy of existing ionospheric models, the ionosphere-free (IF) model has always been the preferred choice for high-precision GNSS positioning users. With the emergence and development of multi-frequency (MF) and multi-GNSS technology, the undifferenced and uncombined (UU) model has been increasingly attractive in recent years [12–14]. Compared with the IF model, the UU model not only reduces the observation noise but also preserves ionospheric information. This model has the ability to provide high-quality original observables for ionospheric modeling [2,15]. Additionally, the UU-PPP based on the priori ionospheric constraint has the potential to reduce the initialization time and avoid re-convergence in the environment with missing signals [15,16]. Up to now, most of the research on BDS PPP has focused on multi-GNSS combined positioning, post-processing positioning, and RT positioning using PPP-B2b corrections [17–19]. Compared with the PPP-B2B-enhanced RT PPP that only serves China and surrounding areas, the RTS-enhanced RT PPP has global service capabilities and is more conducive to the global application and promotion of BDS. However, there is limited study related to BDS-only RT PPP driven by RTS products. More importantly, almost all BDS-related RT PPP users

only adopt the DF IF model, and research on the performance of the DF UU model using BDS-only observations is missing. Thus, the global performance of BDS-2 and BDS-3 joint RT UU-PPP using RTS products from five ACs was investigated for the first time. It is worth noting that RTS vertical total electron content (VTEC) products as priori ionospheric constraints are adopted for RT UU-PPP, and the optimal BDS RT positioning performance could be achieved in this study. Moreover, the differences in positioning accuracy and convergence between the RT UU-PPP and RT IF-PPP for BDS-2+3 were also discussed with extensive datasets.

The arrangement of this paper is as follows: the evaluation method of the RTS orbit and clock accuracy and the mathematical models of BDS-2+3 RT UU-PPP are introduced in the next section. Then, the experimental datasets and processing strategies are summarized. The evaluation results of different RTS products and some key indicators of positioning performance are discussed in part four. Finally, some new findings and conclusions are presented in brief.

2. Methods

This section is mainly divided into two parts. One is the evaluation method of RTS orbit and clock products in comparison with final precise products. Another is the mathematical model of BDS-2 and BDS-3 joint RT PPP.

2.1. RTS Orbits and Clocks Recovery

The format of the RTS orbits and clocks is completely different from IGS's final precise products and needs to be recovered by legacy broadcast ephemeris and SSR corrections. The satellite coordinates calculated from the broadcast ephemeris are located in the earth-centered earth-fixed (ECEF) coordinate system, which can be denoted as $(X^s_{brd}, Y^s_{brd}, Z^s_{brd})^{\mathrm{T}}$, while SSR corrections of orbit are based on the satellite-fixed coordinate system and expressed as satellite position corrections $(\delta R, \delta A, \delta C)^{\mathrm{T}}$ and satellite velocity corrections $(\delta \dot{R}, \delta \dot{A}, \delta \dot{C})^{\mathrm{T}}$. Consequently, the RTS orbits $(X^s_{rts}, Y^s_{rts}, Z^s_{rts})^{\mathrm{T}}$ can be obtained from [6]

$$\begin{bmatrix} X^s_{rts} \\ Y^s_{rts} \\ Z^s_{rts} \end{bmatrix} = \begin{bmatrix} X^s_{brd} \\ Y^s_{brd} \\ Z^s_{brd} \end{bmatrix} - Z \cdot \left(\begin{bmatrix} \delta R \\ \delta A \\ \delta C \end{bmatrix} + \begin{bmatrix} \delta \dot{R} \\ \delta \dot{A} \\ \delta \dot{C} \end{bmatrix} \cdot (t - t_0) \right) \tag{1}$$

With

$$Z = \begin{bmatrix} \frac{\dot{r}}{|\dot{r}|} \times \frac{r \times \dot{r}}{|r \times \dot{r}|} \\ \frac{\dot{r}}{|\dot{r}|} \\ \frac{r \times \dot{r}}{|r \times \dot{r}|} \end{bmatrix} \tag{2}$$

where t and t_0 denote calculated time and reference time, respectively. Z is the coordinate transformation matrix. r and $\dot{r}$ denote satellite position vector and satellite velocity vector, respectively.

For SSR corrections of the clock, three polynomial coefficients (A_0, A_1, A_2) are given to calculate the satellite clock correction. The RTS clocks dt^s_{rts} can be expressed as [6]

$$dt^s_{rts} = dt^s_{brd} + \frac{A_0 + A_1(t - t_0) + A_2(t - t_0)^2}{c} \tag{3}$$

where dt^s_{brd} is the broadcast clocks. c is the speed of light.

2.2. Quality Assessment of Recovered RTS Orbits and Clocks

To measure the accuracy of RTS products provided by different ACs, the GBM (Geodetic Benchmark Multi-GNSS) final orbits and clocks can be selected as references. The RTS orbit and clock errors can be expressed as

$$\begin{bmatrix} \Delta R \\ \Delta A \\ \Delta C \end{bmatrix} = Z^{\mathrm{T}} \cdot \left(\begin{bmatrix} X^s_{rts} \\ Y^s_{rts} \\ Z^s_{rts} \end{bmatrix} - \begin{bmatrix} X^s_{gbm} \\ Y^s_{gbm} \\ Z^s_{gbm} \end{bmatrix} \right) \tag{4}$$

$$\Delta t^s = dt^s_{rts} - dt^s_{gbm} \tag{5}$$

where $(\Delta R, \Delta A, \Delta C)^{\mathrm{T}}$ is the RTS orbit errors in the satellite-fixed coordinate system. $(X^s_{gbm}, Y^s_{gbm}, Z^s_{gbm})^{\mathrm{T}}$ is the GBM precise orbits in the ECEF coordinate system. Δt^s is the RTS clock errors. dt^s_{gbm} is the GBM precise clocks.

Some necessary handling measures need to be emphasized. (1) Since the data sampling intervals of SSR corrections and broadcast ephemeris are not consistent, the issue of data (IOD) parameter is used to match the above two types of data, and the specific matching method for BDS satellites can be referred to [9]. (2) The majority of RTS orbits refer to the phase center of the satellite antenna, but GBM orbits are based on the center of satellite mass. Thus, the satellite antenna file needs to be adopted for correction of phase center offset (PCO). It should be noted that the satellite phase center of RTS orbits for the five selected ACs is based on the L1 frequency rather than the DF ionospheric combination. (3) The GNSS-specific time scale of different ACs has an apparent discrepancy and the time benchmark of RTS clocks is not consistent with the GBM clocks. In order to remove these systematic biases before comparing clock errors, the median of RTS-minus-GBM satellite clocks for all satellites at each epoch can be deducted from the clock errors of each satellite [8]. The flowchart for evaluating the accuracy of RTS products is shown in Figure 1.

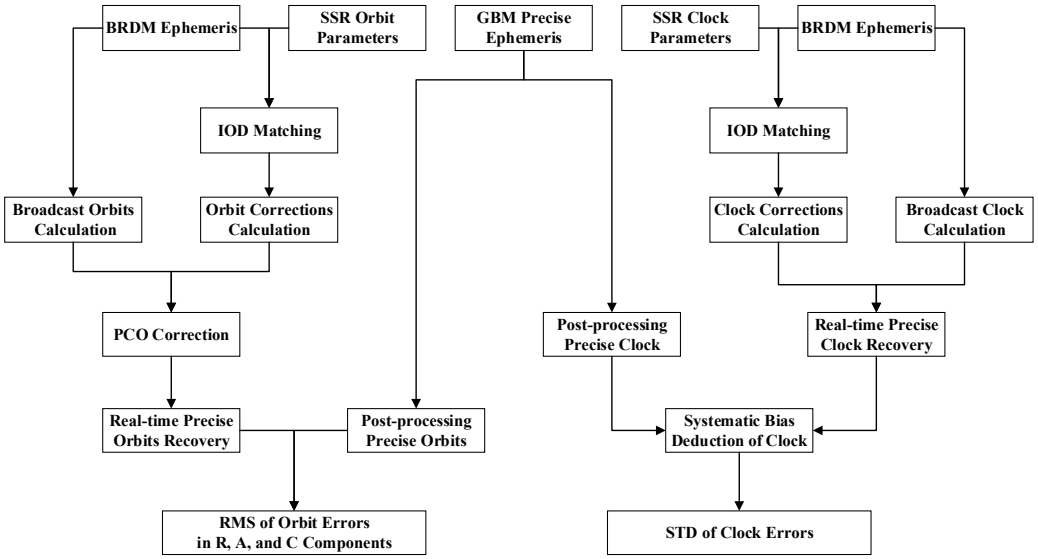

Figure 1. Flowchart of RTS orbits and clocks accuracy evaluation.

2.3. BDS-2 and BDS-3 Joint Real-Time Undifferenced and Uncombined PPP

The raw observations of code $P^s_{r,i}$ and phase $L^s_{r,i}$ for BDS can be expressed as [20]

$$\begin{cases} P^s_{r,i} = \rho^s_{r,i} + c \cdot (dt_r - dt^s) + T^s_r + \mu_i \cdot I^s_{r,1} + B_{r,i} - B^{s,i} + \varepsilon^s_{P,i} \\ L^s_{r,i} = \rho^s_{r,i} + c \cdot (dt_r - dt^s) + T^s_r - \mu_i \cdot I^s_{r,1} + \lambda^s_i \cdot N^s_{r,i} + b_{r,i} - b^{s,i} + \varepsilon^s_{L,i} \end{cases} \tag{6}$$

where indices s and r denote the satellite and GNSS receiver, respectively; i is the frequency number; $\rho_{r,i}^{s}$ is the geometric distance from the GNSS receiver to the satellite; dt_r and dt^s denote the receiver clock offset and satellite clock offset, respectively; T_r^s is the slant tropospheric delay error; $I_{r,1}^{s}$ is the slant ionospheric delay error on the first frequency; $\mu_i^Q = \left(f_1^s / f_i^s\right)^2$ is the frequency conversion factor and f_i^s denotes the frequency of the BDS signal; $N_{r,i}^{s}$ is the integer ambiguity of phase observation; λ_i^s is the wavelength of phase observation; $B^{s,i}$ and $B_{r,i}$ are the code hardware delays at the satellite and GNSS receiver end, respectively; $b^{s,i}$ and $b_{r,i}$ are the phase hardware delays at the satellite and GNSS receiver end, respectively; and $\varepsilon_{P,i}^{s}$ and $\varepsilon_{L,i}^{s}$ are the code and phase observation noises including the multipath error, respectively.

The GBM precise clocks cannot be directly used for the BDS UU-PPP because these clocks are obtained from the B1I and B3I IF observations. The BDS code hard delays need to be applied to correct the satellite and receiver clock offsets as follows,

$$\begin{cases} \overline{dt}^{s} = dt^{s} + \frac{d_{IF}^{s}}{c} \\ \overline{dt}_r = dt_r + \frac{d_{r,IF}}{c} \end{cases} \tag{7}$$

where $\overline{dt}^{s}$ and $\overline{dt}_r$ denote the actual clock offsets of the satellite and receiver, respectively. d_{IF}^{s} and $d_{r,IF}$ denote the IF code hardware delays of the BDS satellite and receiver, respectively, which can be obtained from

$$\begin{cases} d_{IF}^{s} = \alpha \cdot B^{s,1} + \beta \cdot B^{s,3} \\ d_{r,IF} = \alpha \cdot B_{r,1} + \beta \cdot B_{r,3} \end{cases} \tag{8}$$

with

$$\begin{cases} \alpha = \frac{(f_1^s)^2}{(f_1^s)^2 - (f_3^s)^2} \\ \beta = \frac{-(f_3^s)^2}{(f_1^s)^2 - (f_3^s)^2} \end{cases} \tag{9}$$

Thanks to the ability of RTS products to provide SSR code bias, the differential code bias (*DCB*) errors can be corrected in the RT UU-PPP. The satellite and receiver *DCB* can be represented as

$$\begin{cases} DCB^{s} = B^{s,1} - B^{s,3} \\ DCB_r = B_{r,1} - B_{r,3} \end{cases} \tag{10}$$

When substituting Equations (7)–(10) into Equation (6), the new observation equations of BDS UU-PPP can be expressed as

$$\begin{cases} P_{r,i}^{s} = \rho_{r,i}^{s} + c \cdot (\overline{dt}_r - \overline{dt}^{s}) + T_r^s + \mu_i \cdot \overline{I}_{r,1}^{s} + \varepsilon_{P,i}^{s} \\ L_{r,i}^{s} = \rho_{r,i}^{s} + c \cdot (\overline{dt}_r - \overline{dt}^{s}) + T_r^s - \mu_i \cdot \overline{I}_{r,1}^{s} + \lambda_i^s \cdot \overline{N}_{r,i}^{s} + \varepsilon_{L,i}^{s} \end{cases} \tag{11}$$

with

$$\begin{cases} \overline{I}_{r,1}^{s} = I_{r,1}^{s} + \beta \cdot (DCB_r - DCB^{s}) \\ \lambda_i^s \cdot \overline{N}_{r,i}^{s} = (\lambda_i^s \cdot N_{r,i}^{s} + b_{r,i} - b^{s,i}) + (d_{r.IF} - d_{IF}^{s}) + \mu_i \cdot \beta \cdot (DCB_r - DCB^{s}) \end{cases} \tag{12}$$

where $\overline{I}_{r,1}^{s}$ is the re-parameterized ionospheric delay. $\overline{N}_{r,i}^{s}$ is the re-parameterized phase ambiguity and has lost its integer property.

BDS-2 and BDS-3, as two generations of BDS systems, serve users in the Asia–Pacific region and on the global scale, respectively. The number of available monitoring stations for tracking BDS-2 and BDS-3 satellites is inconsistent, and the process strategies of RTS products for the two systems are also different. Therefore, the intra-system bias (ISB) between BDS-2 and BDS-3 should be considered in the positioning when using all BDS satellites [21]. Since the number of BDS-3 satellites is significantly superior to BDS-2 satellites, the receiver clock offset of BDS-3 is set as the reference, and the ISB parameters are applied to the BDS-2 satellites in this study. Considering that the UU-PPP performance can be improved by

introducing the external ionospheric constraint, the RTS VTEC products with excellent accuracy are used in the RT UU-PPP [16]. To sum up, the linearized observation equations for the code and phase of BDS-2 and BDS-3 joint UU-PPP based on the RTS VTEC constraints can be expressed as

$$\begin{cases} P_{r,i}^{s,C2} = \mathbf{e}_r^s \cdot \mathbf{g} + c \cdot (d\bar{t}_r - d\bar{t}^s) + ISB + M \cdot T_{zwd} + \mu_i \cdot \bar{I}_{r,1}^s + \varepsilon_{P,i}^s \\ P_{r,i}^{s,C3} = \mathbf{e}_r^s \cdot \mathbf{g} + c \cdot (d\bar{t}_r - d\bar{t}^s) + M \cdot T_{zwd} + \mu_i \cdot \bar{I}_{r,1}^s + \varepsilon_{P,i}^s \\ L_{r,i}^{s,C2} = \mathbf{e}_r^s \cdot \mathbf{g} + c \cdot (d\bar{t}_r - d\bar{t}^s) + ISB + M \cdot T_{zwd} - \mu_i \cdot \bar{I}_{r,1}^s + \lambda_i^s \cdot \bar{N}_{r,i}^s + \varepsilon_{L,i}^s \\ L_{r,i}^{s,C3} = \mathbf{e}_r^s \cdot \mathbf{g} + c \cdot (d\bar{t}_r - d\bar{t}^s) + M \cdot T_{zwd} - \mu_i \cdot \bar{I}_{r,1}^s + \lambda_i^s \cdot \bar{N}_{r,i}^s + \varepsilon_{L,i}^s \\ \chi = \bar{I}_{r,1}^s + \varepsilon_\chi^s \end{cases} \tag{13}$$

where indices $C2$ and $C3$ denote the BDS-2 and BDS-3 satellites, respectively; $\mathbf{e}_r^s$ represents the unit vector of the component between the receiver and satellite; $\mathbf{g}$ denotes the vector of the receiver coordinate errors in three directions; M is the tropospheric mapping function; T_{zwd} is the zenith wet delay (ZWD) of tropospheric errors; χ is the virtual observation equation of the ionospheric errors; and ε_χ^s is the noise of virtual ionospheric observation.

In the process of exploring the global BDS-2 and BDS-3 joint RT UU-PPP performance, twenty multi-GNSS experiment (MGEX) stations distributed around the world were used for positioning experiments in this study. To accurately set prior constraints for testing stations at different locations, the widely used spatial-temporal constraint method is adopted. The variance of ionospheric parameters can be expressed as [16]

$$\sigma_{iono}^2 = \begin{cases} \Omega_f \cdot [\sigma_0^2 + \sigma_1^2 \cdot \cos(\omega) \cos(\frac{T_l - 14}{12} \pi)], & \omega < \frac{\pi}{3} \text{ or } 8 < T_l < 20 \\ \Omega_f \cdot \sigma_0^2, & otherwise \end{cases} \tag{14}$$

$$\Omega_f = \frac{(R_e + h_{iono})}{R_e(1 - \sin^2\theta) + h_{iono}} \tag{15}$$

where R_e is the average radius of the Earth (6371 km); h_{iono} is the height of the ionospheric shell (450 km for RTS VTEC); θ is the zenith angle; σ_0^2 and σ_1^2 can be set as 0.25 m^2, which are the variance of the ionospheric delay and variation, respectively; ω is the latitude of the IPP (Ionospheric Pierce Point) in degrees; and T_l is the local time (LT) in hours.

The estimable parameters Π of the BDS-2 and BDS-3 joint RT UU-PPP can be summarized as

$$\Pi = [\mathbf{g}, d\bar{t}_r, ISB, T_{zwd}, \bar{I}_{r,1}^s, \bar{N}_{r,i}^s] \tag{16}$$

3. Experiment Datasets and Processing Strategies

The information on RTS products and MGEX stations was described first, and the processing strategies in the positioning domain were depicted in detail.

3.1. Experiment Datasets

BDS SSR corrections of five ACs from DoY (Day of Year) 305 to 316 in 2022 are received through the Internet, and the corresponding GBM products are set as references. The comparison interval for orbit and clock errors are set to 5 min and 30 s, respectively. The details of different RTS products for BDS are shown in Table 1. As for the experiment of BDS-2 and BDS-3 joint RT UU-PPP, the BDS observations of twenty MGEX stations with 30 s sampling for 12 days (DoY 305–316 in 2022) are selected and their distribution is presented in Figure 2.

Table 1. Information on BDS RTS products of each AC.

ACs	Mount Point	Update Interval (Orbit/Clock)	Number of BDS Satellites	Missing BDS Satellites
CAS (Chinese Academy of Sciences)	SSRA00CAS1	5 s/5 s	37	\
CNES (Centre National d'Etudes Spatiales)	SSRA00CNE0	5 s/5 s	36	C21
GFZ (Deutsches GeoForschungsZentrum)	SSRA00GFZ0	5 s/5 s	37	\
SHAO (Shanghai Astronomical Observatory)	SSRA01SHA0	30 s/30 s	31	C11–12, C14, C23–24, C27
WHU (Wuhan University)	SSRA00WHU0	5 s/5 s	31	C11, C14, C16, C27–28, C39

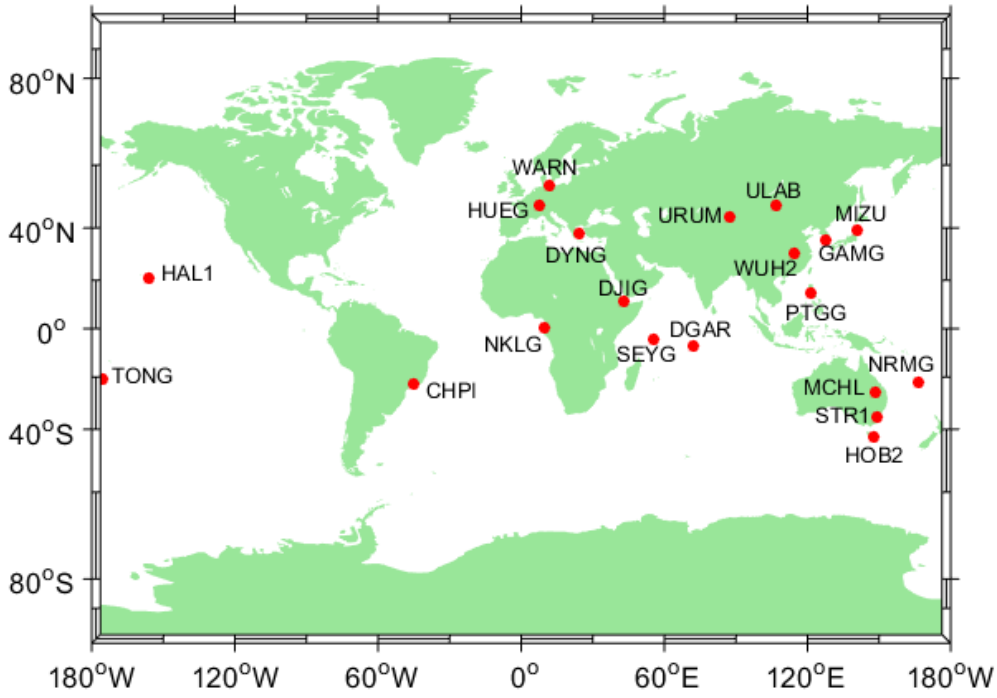

Figure 2. Distribution of the tested 20 MGEX stations.

3.2. Processing Strategies

The code and phase observations of B1I and B3I with the interval of 30 s are used to carry out BDS-2 and BDS-3 joint RT UU-PPP. The priori precisions of code and phase are set as 30 cm and 3 mm, respectively. Since the BDS pseudo-range bias could degrade the performance of BDS-2 and BDS-3 joint PPP and the accuracy of RTS products for BDS-2 is generally inferior to that for BDS-3, the weight of BDS-2 observations has to be reduced [22,23]. In this study, for CAS, CNES, GFZ, SHAO, and WHU RTS products, the weights of BDS-2 observations are set as 1/3, 1/10, 1/5, 1/5, and 1/15 of BDS-3 observations with extensive positioning tests, respectively. The elevation-dependent weighting method of [24] is adopted for setting variances of the stochastic model. The precise positions of MGEX stations can be derived from the weekly solution of Solution INdependent EXchange (SINEX). The main correction models and process strategies of BDS-2 and BDS-3 joint RT UU-PPP are summarized in Table 2. In addition, the earth rotation, relativistic effect, tidal correction, and phase windup must also be corrected through relevant models.

Table 2. Correction models and strategies of BDS-2 and BDS-3 joint RT UU-PPP.

Items	Processing Strategies
Elevation cutoff angle	7°
Satellite orbits and clocks	Broadcast ephemeris [25] + SSR corrections
Satellites DCB	SSR code bias
PCO and phase center variation (PCV)	Corrected with ATX file (igs14_2233.atx)
Tropospheric delay	Corrected by GPT2w + SAAS + VMF (Dry component) and estimated as random-walk noise (Wet component) [20]
Ionospheric delay	Corrected by CNES RT-VTEC products and estimated as random-walk noise [16]
Estimator	Kalman filter
Receiver coordinates and clocks	Estimated as white noise
ISB	Estimated as random-walk noise [20]
Phase ambiguities	Estimated as float solution

4. Results and Discussions

First of all, the quality of RTS orbits and clocks for different ACs was evaluated and compared. Then, the static and kinematic positioning performance of BDS-2 and BDS-3 joint RT UU-PPP was investigated and compared with corresponding RT IF-PPP solutions. Two key indicators of positioning accuracy and convergence time were used for the quantitative analysis.

4.1. Accuracy Analysis of RTS Products from Different ACs

The RMS of orbit errors and STD of clock errors for each BDS satellite from five ACs are presented in Figure 3. "CNE" and "SHA" are abbreviations for CNES and SHAO, respectively. The results of the BDS-2 satellites (C06–C16) and BDS-3 satellites (C19–C46) are depicted on the left and right sides of the solid black line, respectively. The blue and green bar charts denote the IGSO and MEO satellites, respectively. The orbit errors exceeding 1.5 m in any direction are considered as gross errors and need to be removed in assessment, while for clock evaluation, the gross error is defined as 3.0 ns. It should be noted that the GEO satellites (C01–05) of BDS are excluded from this study. One reason is that the orbit and clock accuracy of GEO satellites are far inferior to IGSO and MEO satellites, which may generate an adverse impact on RT PPP [8]. Another issue is that GEO satellites are only visible in the Asia–Pacific region, but this contribution mainly focuses on the global positioning performance of BDS. From Figure 3a–c, we can see that the orbit accuracy of MEO satellites is commonly better than that of IGSO satellites in all directions for all ACs. In the radial direction, the MEO orbit accuracy of GFZ, SHAO, and WHU is superior to that of CAS and CNES. The RMS of orbit errors for CAS C23–26 satellites and CNE C25–26 satellites can be up to 20 cm and exceeds that of other MEO satellites by 2 to 4 times. The observation weights of these satellites should be reduced in RT PPP because the positioning performance is highly dependent on the radial error of orbits. The RMS of radial orbit errors for most IGSO satellites is about 10–15 cm, while the corresponding accuracies of GFZ C38, C39, and C40 satellites can reach up to 120.6, 141.3, and 53.3 cm, respectively, and similar gross errors also appear in the along-track and cross-track directions. This may be due to GFZ mistakenly using PCO values of C38–40 satellites when solving the SSR orbit corrections. Therefore, the C38–40 satellites should be excluded from the experiment of GFZ-drive RT PPP in this study. In terms of the along-track orbit errors, the RMS of C23–24, C36–37, and C45–46 satellites for CAS is far higher than that of other MEO satellites and can even be up to 38 cm. Similar situations also occur in the C37 satellite of SHAO. CNES and GFZ have five (C6–8, C16, C38) and three IGSO (C38–40) satellites with along-track orbit accuracy exceeding 30 cm, respectively. By comparison, WHU has the best orbit performance in the along-track direction, and its RMS error for most satellites can be better than 10 cm. There is no significant difference in the accuracy of MEO satellites between the five ACs regarding the cross-track orbit errors. All MEO satellites have stable cross-track

orbit accuracy, but some outliers can be found in the IGSO satellites, such as the CNES C6–8, C16, and C38 satellites.

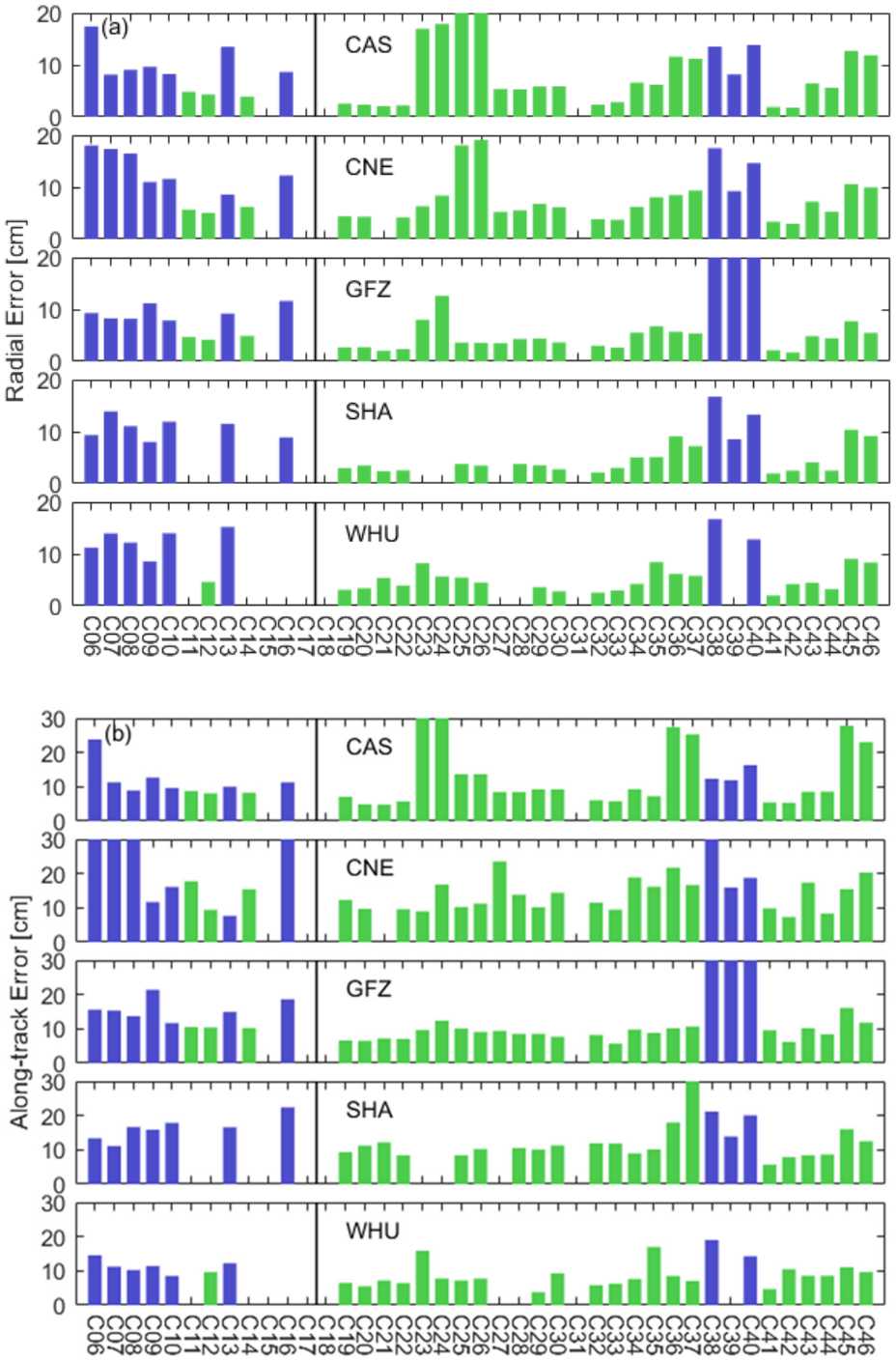

Figure 3. *Cont.*

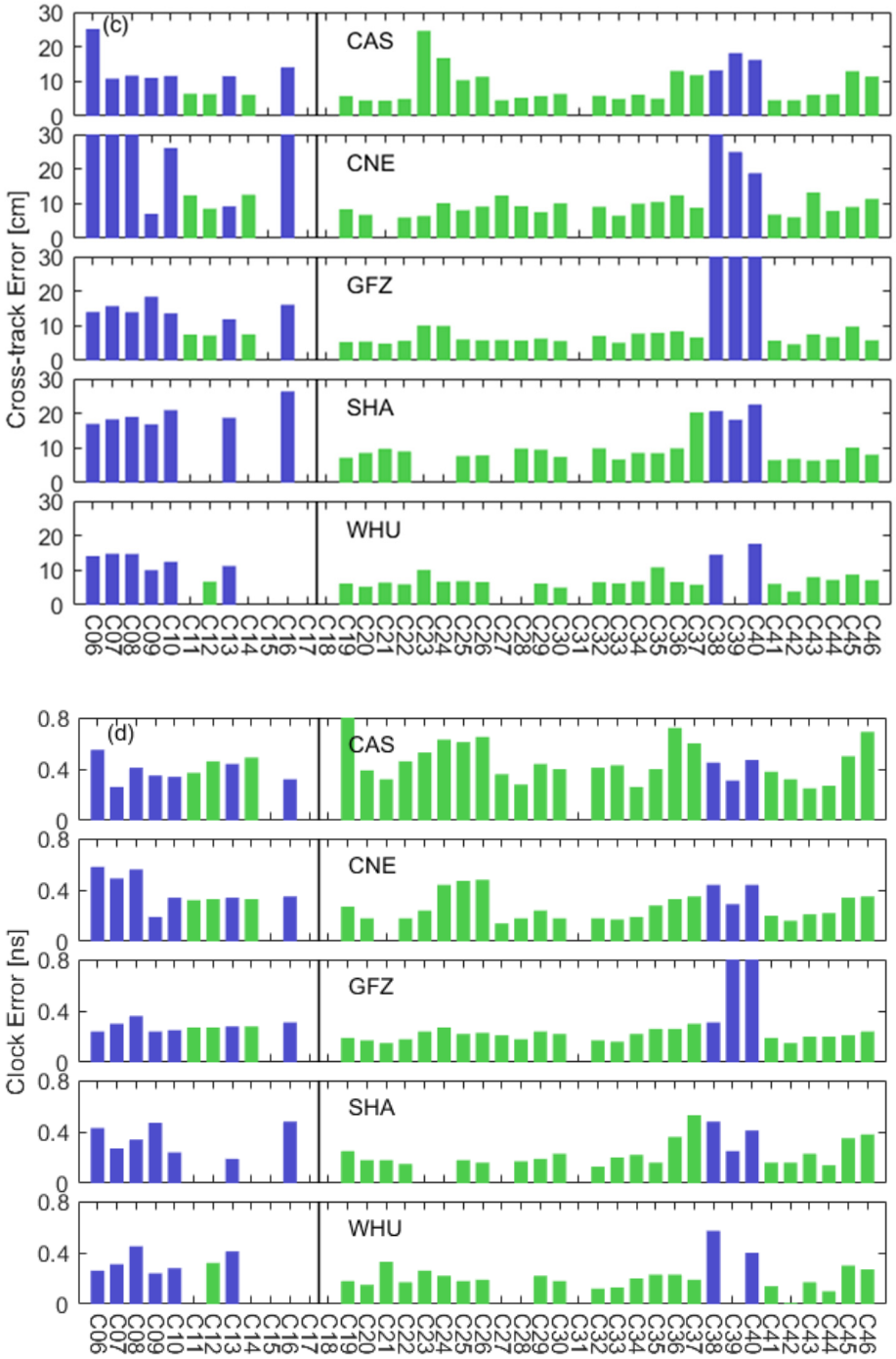

Figure 3. RMS of orbit errors and STD of clock errors for BDS RTS products from five ACs, (**a**) for radial errors of orbit, (**b**) for along-track errors of orbit, (**c**) for cross-track errors of orbit, and (**d**) for clock errors (DoY 305–316, 2022).

As to clock accuracy (see in Figure 3d), the CAS has the worst performance among all ACs, and the STD of clock errors exceeds 0.4 ns for 60% of satellites. Except for C39–40 satellites with an STD of up to 1.4 ns, the clock accuracy of GFZ is comparable to that of SHAO and WHU for all satellites and can be stable within 0.4 ns. If both MEO and IGSO satellites are considered, SHAO and WHU have similar and the best clock accuracy.

According to the property and service stage of satellites, all BDS satellites can be divided into four parts, including IGSO (C06–10, C13, C16, C38–40), MEO (C11–12, C14, C19-C30, C32–37, C41–46), BDS-2 (C6–14, C16), and BDS-3 (C19–30, C32–46) satellites. The

mean RMS of orbit errors and mean STD of clock errors for each part are shown in Figure 4. It is worth noting that the C38–40 satellites of GFZ were defined as outliers and excluded from this assessment. We can see that the orbit accuracy decreases sequentially from the radial (R), cross-track (C), and along-track (A) directions. Regardless of ACs, the orbit accuracy of MEO satellites is superior to that of IGSO satellites in all directions. As for MEO satellites, the mean RMS of radial orbit errors for GFZ, SHAO, and WHU is at the same level with about 4.5 cm, while for CAS and CNES, their mean RMS may increase to over 7 cm. The mean RMS of IGSO orbit errors in the radial direction is about 11–15 cm for all ACs. In terms of the along-track and cross-track orbit errors, the mean RMS of CNES is larger than that of other ACs and is even up to 29.2 and 40.1 cm for IGSO satellites, respectively. Conversely, no matter the IGSO and MEO satellites, the orbit accuracy of WHU in both the along-track and cross-track directions is the best among all ACs. From the perspective of BDS-2 and BDS-3 satellites, the orbit accuracy of BDS-3 satellites is better than that of BDS-2 satellites in all directions. The mean RMS of radial orbit errors for the BDS-3 satellites provided by SHAO and WHU is about 5.5 cm and better than that of GFZ (6.5 cm), CNES (8.0 cm), and CAS (8.6 cm). While for the BDS-2 satellites, the radial orbit accuracy of GFZ is the highest with a mean RMS of 7.9 cm. In the along-track direction, the orbit accuracy of WHU is the best and reaches 11.1 and 9.0 cm for the BDS-2 and BDS-3 satellites, respectively. When it comes to cross-track orbit accuracy for the BDS-2 satellites, CAS, GFZ, and WHU have a similar RMS of about 12 cm, but the corresponding accuracy for the BDS-3 satellites can be improved to no more than 9 cm. Compared with the results of previous research using RTS products in 2021 [8,10], the orbit accuracies of CAS, CNES, GFZ, and WHU are improved at the end of 2022, especially for GFZ products and IGSO satellites.

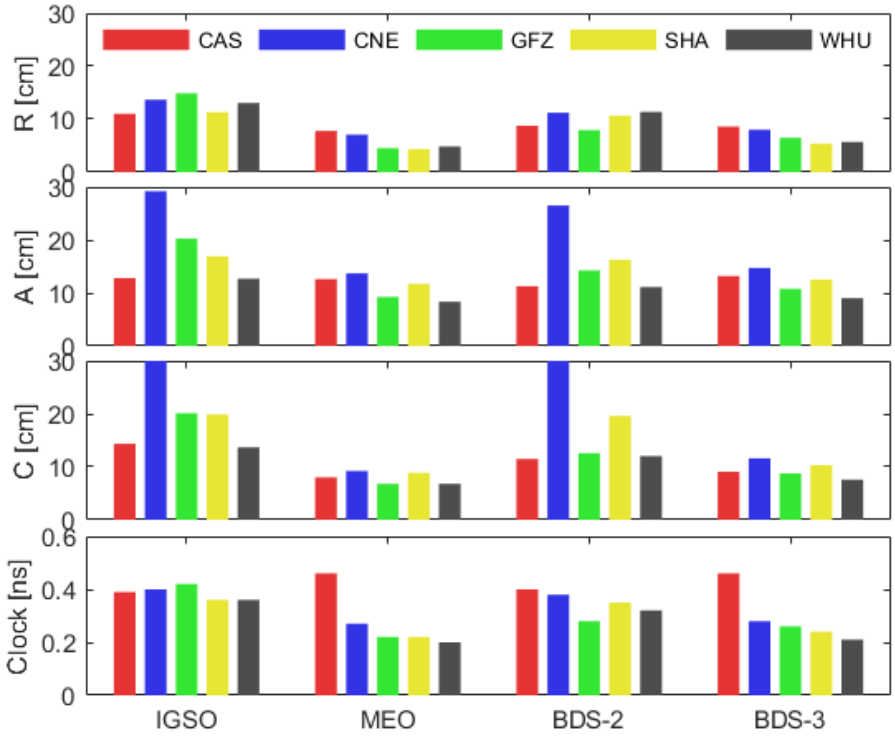

Figure 4. Mean RMS of orbit errors and mean STD of clock errors for all different types of BDS satellites.

In addition to radial orbit errors, the quality of satellite clock errors is closely related to the RT PPP performance. The clock accuracy of IGSO satellites for CAS, CNES, and GFZ is at the same level with a mean RMS of about 0.4 ns, while for SHAO and WHU, the corresponding accuracy can be improved to 0.36 ns. In comparison with IGSO satellites, the mean RMS of MEO clock errors for CNES, GFZ, SHAO, and WHU can be improved

by 32.5%, 47.6%, 38.9%, and 44.4% to 0.27, 0.22, 0.22, and 0.20 ns, respectively. There is an abnormal phenomenon in that the clock accuracy of CAS has decreased from 0.39 ns for IGSO satellites to 0.46 ns for MEO satellites, a decrease of 18.0%. The mean RMS of BDS-2 clock errors is 0.40, 0.38, 0.28, 0.35, and 0.32 ns for CAS, CNES, GFZ, SHAO, and WHU, respectively. Except for CAS, the BDS-3 clock accuracy of other ACs is higher than that of BDS-2 clock accuracy, and its mean RMS of 0.28, 0.26, 0.24, and 0.21 ns can be achieved for CNES, GFZ, SHAO, and WHU, respectively. Compared to the clock accuracy of the BDS-2 (about 0.5 ns) and BDS-3 satellites (about 0.35 ns) in 2021 [8,9], the quality of RTS clock products at the end of 2022 has been improved for both the BDS-2 and BDS-3 satellites.

4.2. Performance of BDS-2 and BDS-3 Joint Real-Time Undifferenced and Uncombined PPP in Static Mode

Figure 5 gives the convergence curves of BDS-2 and BDS-3 joint static RT UU-PPP at the 68% confidence level. To measure the performance of this RT UU-PPP, the time series of convergence for BDS-2 and BDS-3 joint RT IF-PPP in static mode using the same datasets are also displayed. First of all, the absolute positioning errors of 240 daily solutions (20 stations × 12 days) for each epoch are sorted in ascending order. Next, we select a value for each epoch that is lower than 68% of all sorted positioning errors. Finally, the values of each epoch are concatenated in the first 90 min. Please note that the horizontal error denotes the combination of north (N) and east (E) errors. We can see that whether it is UU-PPP or IF-PPP, the convergence speed of the vertical error is generally faster than that of the horizontal error. Since the CAS has the worst clock accuracy among all ACs, especially for MEO satellites, both the horizontal and vertical convergence curves of CAS in RT IF-PPP were significantly higher than those of other ACs during the 10–40 min. However, this situation did not occur in the horizontal component of RT UU-PPP and was not particularly evident in the vertical component. After 40 min, the horizontal convergence curve of all ACs showed good consistency for both UU-PPP and IF-PPP. Thanks to the great orbit and clock accuracies of WHU, after converging to 0.2 m, its convergence curve always remains at the best level in the horizontal and vertical components of both UU-PPP and IF-PPP.

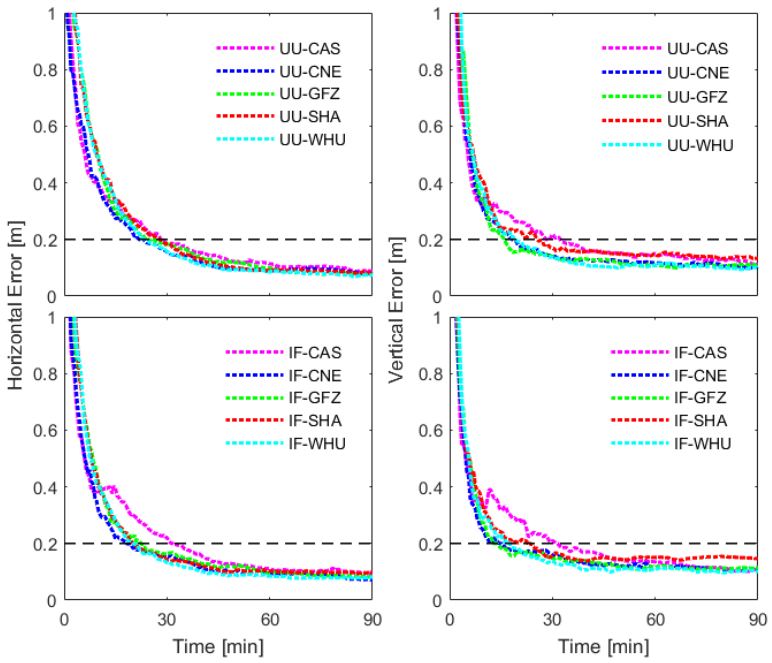

Figure 5. Time series of convergence for BDS-2 and BDS-3 joint RT UU-PPP and RT IF-PPP in static mode at the 68% confidence level (20 MGEX stations, DoY 305–316, 2022).

In order to quantitatively analyze the specific convergence time of different static RT PPP solutions, the convergence criterion is defined as the time when the above conver-

gence curve is below 0.2 m, and the statistical results of each AC are shown in Figure 6. Due to the lower clock accuracy of MEO satellites for CAS compared to other ACs, the convergence time of CAS-drive RT IF-PPP is the longest in both the horizontal and vertical components and exceeds 30 min. With the introduction of CNES RT-VTEC constraints, the horizontal convergence time of CAS-drive RT UU-PPP can be improved by 10.9% to 28.5 min. However, this phenomenon of external ionospheric constraints improving convergence performance did not appear in the results of other ACs. The main reason is that the accuracy of CNES RT-VTEC products is limited and cannot precisely eliminate ionospheric errors like the IF-PPP model. If the external ionospheric model is accurate enough, the convergence speed of UU-PPP is fully capable of surpassing that of IF-PPP [26]. The difference in convergence time between UU-PPP and IF-PPP for all ACs is summarized in Table 3. We can see that SHAO has the maximum decline rates in horizontal convergence time and is up to 36.6% from 20.5 min of RT IF-PPP to 28.0 min of RT UU-PPP, while for the vertical convergence time, the maximum decline rate appears in the results of CNES, which does not exceed 20%. Only focusing on RT UU-PPP, the horizontal convergence time of CAS and SHAO is about 28 min and worse than that of other ACs with no more than 25 min. There are apparent differences in the vertical convergence time among different ACs. CNES, GFZ, and WHU are in the first level and less than 20 min. CAS and SHAO have relatively long vertical convergence times of over 32 and 25 min, respectively.

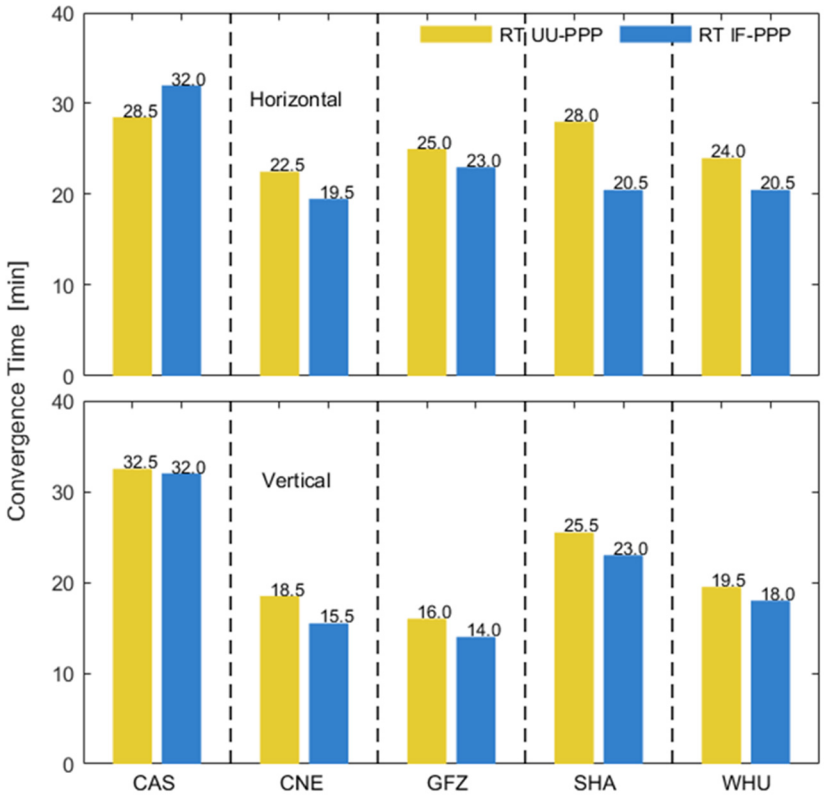

Figure 6. Convergence time of different ACs for BDS-2 and BDS-3 joint RT UU-PPP and RT IF-PPP in static mode when positioning errors converge to 0.2 m (20 MGEX stations, DoY 305–316, 2022).

Table 3. Decline rates of the convergence speed for RT UU-PPP compared to RT IF-PPP in static mode (unit: %).

Component	CAS	CNE	GFZ	SHA	WHU
Horizontal	−10.9	15.4	8.7	36.6	17.1
Vertical	1.6	19.4	14.3	10.9	8.3

The positioning errors after 2 h in the daily solution are collected to calculate the RMS positioning accuracy. In total, 240 daily RMS values can be obtained from 20 MGEX stations in the period of DoY 305–316. The boxplot of the RMS positioning accuracy for BDS-2 and BDS-3 joint RT UU-PPP and RT IF-PPP in static mode is shown in Figure 7, and the numbers in this figure denote the median of all RMS values. The red plus sign "+" in Figure 7 represents outlier. It should be noted that 2D (two-dimensional) represents the horizontal component, and 3D (three-dimensional) represents the combination of N, E, and U (up) errors. We can see that the positioning accuracy of the N component is significantly better than that of the E component for all ACs regardless of RT UU-PPP or RT IF-PPP. The RMS of both N and E positioning errors for CAS is clearly larger than that for other ACs, which is caused by the poor quality of CAS clock products, but it has no impact on the U component. GFZ has the worst positioning accuracy in the U component with a median RMS of about 8.5 cm. Except for CAS, the horizontal positioning accuracy of other ACs is at the same level and can be better than 4 cm. There are no evident differences in 3D positioning accuracy between all ACs, whose median RMS is no more than 10 cm. Taking the static RT IF-PPP as references, the improvement rates of positioning accuracy of RT UU-PPP for different ACs are summarized in Table 4. With the help of CNES RT-VTEC constraints, RT UU-PPP has slightly better positioning accuracy in both horizontal and vertical components after convergence. The main reason is that the observation noise of UU-PPP is lower than that of IF-PPP and the ionospheric errors can be completely removed since the ionospheric parameters are estimated very accurately after convergence. For different ACs, the 3D positioning accuracy of RT UU-PPP can only be improved by 2.0% to 8.7% in comparison with RT IF-PPP in static mode.

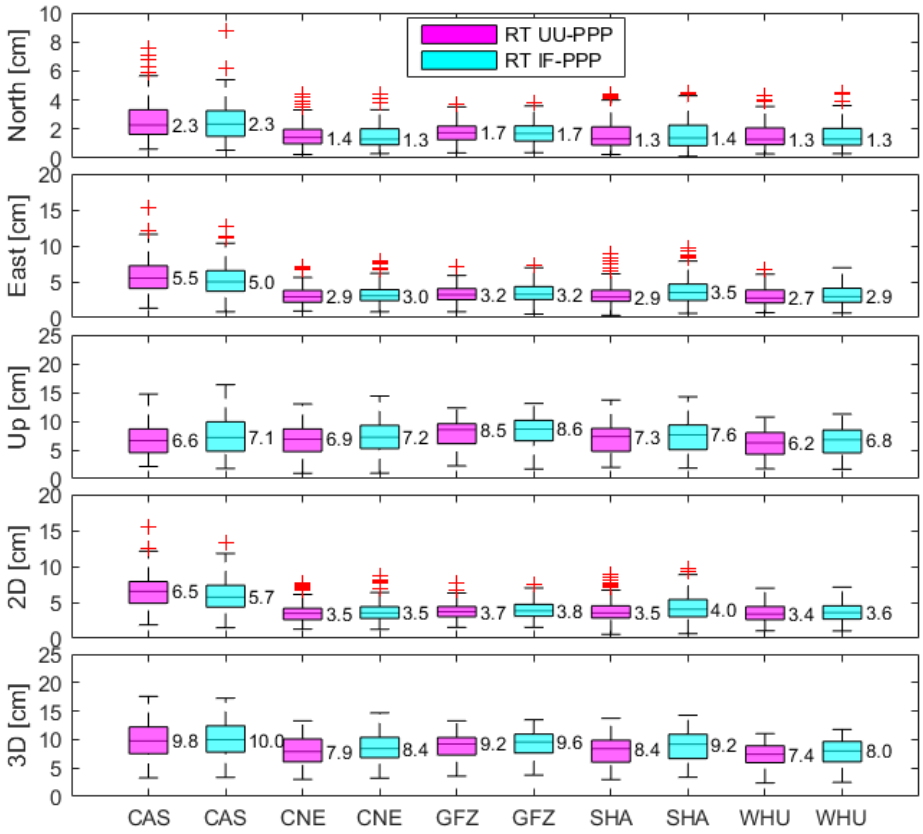

Figure 7. Distribution of RMS positioning accuracy for BDS-2 and BDS-3 joint RT UU-PPP and RT IF-PPP in static mode (20 MGEX stations, DoY 305–316, 2022).

Table 4. Improvement rates of median RMS positioning accuracy for RT UU-PPP compared to RT IF-PPP in static mode (unit: %).

Component	CAS	CNE	GFZ	SHA	WHU
Horizontal	−14.0	0.0	2.6	12.5	5.6
Vertical	7.0	4.2	1.2	3.9	8.8
3D	2.0	6.0	4.2	8.7	7.5

4.3. Performance of BDS-2 and BDS-3 Joint Real-Time Undifferenced and Uncombined PPP in Kinematic Mode

Using statistical methods similar to static RT PPP, the convergence curves of BDS-2 and BDS-3 joint kinematic RT UU-PPP and RT IF-PPP at the 68% confidence level can be seen in Figure 8. Different from the vertical convergence curves, the convergence curves of the horizontal component for all ACs have good consistency in both RT UU-PPP and RT IF-PPP. The horizontal positioning errors of all ACs can be less than 0.2 m after around 60 min. The vertical convergence curve of CAS in RT IF-PPP is higher than that of other ACs during the 10–30 min, which is caused by the worse accuracy of CAS clock products. However, the corresponding convergence performance in RT UU-PPP can be substantially improved by adopting the CNES RT-VTEC constraints. As for RT UU-PPP, CNES exhibits the slowest convergence speed in the vertical component, which may be related to the worst IGSO orbit accuracy of CNES. It is important to note that the vertical convergence performance of SHAO is optimal in most periods regardless of UU-PPP or IF-PPP.

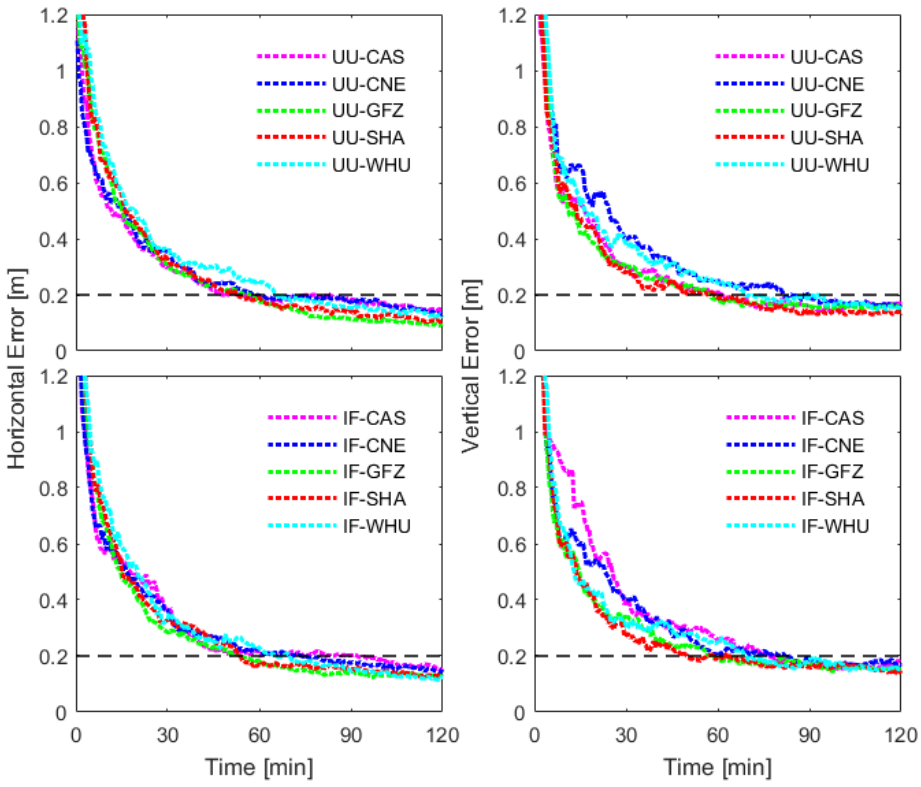

Figure 8. Time series of convergence for BDS-2 and BDS-3 joint RT UU-PPP and RT IF-PPP in kinematic mode at the 68% confidence level (20 MGEX stations, DoY 305–316, 2022).

Figure 9 shows the convergence time of BDS-2 and BDS-3 joint RT UU-PPP and RT IF-PPP in kinematic mode for all ACs when positioning errors converge to 0.2 m. Compared with static RT PPP, the convergence time of kinematic RT PPP in both the horizontal and vertical components has increased by at least 2 times. In this kinematic case of poor convergence performance, the convergence time of RT UU-PPP can be shortened

through CNES RT-VTEC constraints, especially for the CAS solutions with relatively longer convergence times. The main reason is that the ionospheric errors of UU-PPP can be precisely calculated, thereby achieving the same effect as the IF-PPP model. Meanwhile, the observation noise of UU-PPP is much smaller than that of IF-PPP, which is beneficial for fast convergence. Table 5 summarizes the improvement rates of the convergence speed for RT UU-PPP compared to RT IF-PPP in kinematic mode. It can be seen that the horizontal and vertical convergence time of CAS-drive RT UU-PPP can be improved by 31.7% and 22.9%, respectively. Such a significant increase also appears in the horizontal convergence time of CNES. Interestingly, the adoption of CNES RT-VTEC constraints has little positive effect on the convergence performance of GFZ-, SHAO-, and WHU-drive RT UU-PPP in both the horizontal and vertical components. This may be due to the limited accuracy of CNES RT-VTEC products. If more precise ionospheric models like global ionospheric maps (GIMs) are used, the convergence speed of RT UU-PPP may be further improved. In terms of RT UU-PPP, the convergence time of CAS, GFZ, and SHAO is at the same level, with about 55 min in the horizontal and 60 min in the vertical, while for the horizontal component of WHU and the vertical component of CNES, their convergence time is significantly longer than other ACs.

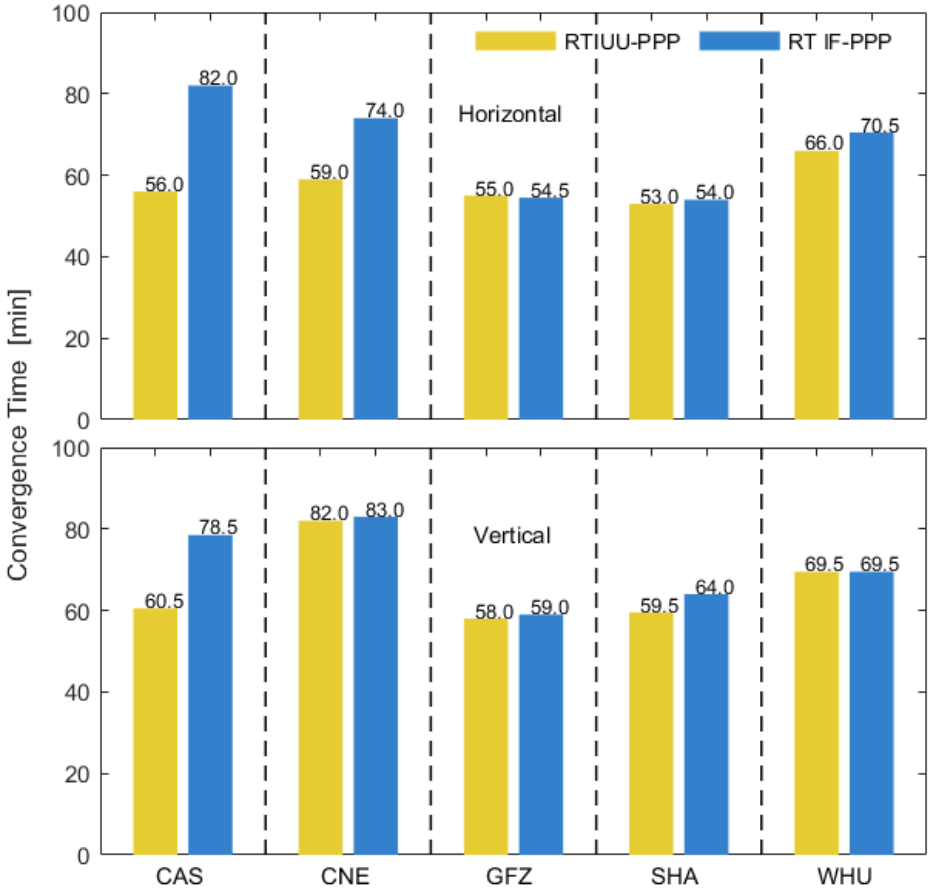

Figure 9. Convergence time of different ACs for BDS-2 and BDS-3 joint RT UU-PPP and RT IF-PPP in kinematic mode when positioning errors converge to 0.2 m (20 MGEX stations, DoY 305–316, 2022).

Table 5. Improvement rates of the convergence speed for RT UU-PPP compared to RT IF-PPP in kinematic mode (unit: %).

Component	CAS	CNE	GFZ	SHA	WHU
Horizontal	31.7	20.3	−0.9	1.9	6.4
Vertical	22.9	1.2	1.7	7.0	0.0

Consistent with the statistical method for positioning accuracy in static RT PPP, the boxplot of RMS positioning accuracy for BDS-2 and BDS-3 joint kinematic RT UU-PPP and RT IF-PPP solutions is shown in Figure 10. As expected, CAS has the worst positioning accuracy among all ACs under the influence of poor clock quality, with median RMS in the horizontal and vertical components of approximately 14 and 19 cm, respectively. While for other ACs, the horizontal and vertical positioning accuracy can be better than 9 and 14 cm, respectively. Except for CAS, there is not much difference in the positioning accuracy among different ACs. By comparison, SHAO has the best positioning accuracy, and its median RMS can achieve 7 and 10 cm in the horizontal and vertical components, respectively. Table 6 summarizes the improvement rates of positioning accuracy for RT UU-PPP compared to RT IF-PPP in the kinematic mode. It can be seen that the application of CNES RT-VTEC constraints has a limited impact on improving the positioning accuracy of RT UU-PPP; the maximum improvement rate of 3D components only reaches 8.2%. The 3D positioning accuracy of WHU has even slightly decreased by 1.4% in RT UU-PPP. At present, the kinematic cm level accuracy can only be achieved in the horizontal component, and the 3D positioning accuracy is around 15 cm for most ACs. It is noteworthy that BDS-2 and BDS-3 joint kinematic RT PPP using RTS products still cannot obtain cm level vertical positioning accuracy.

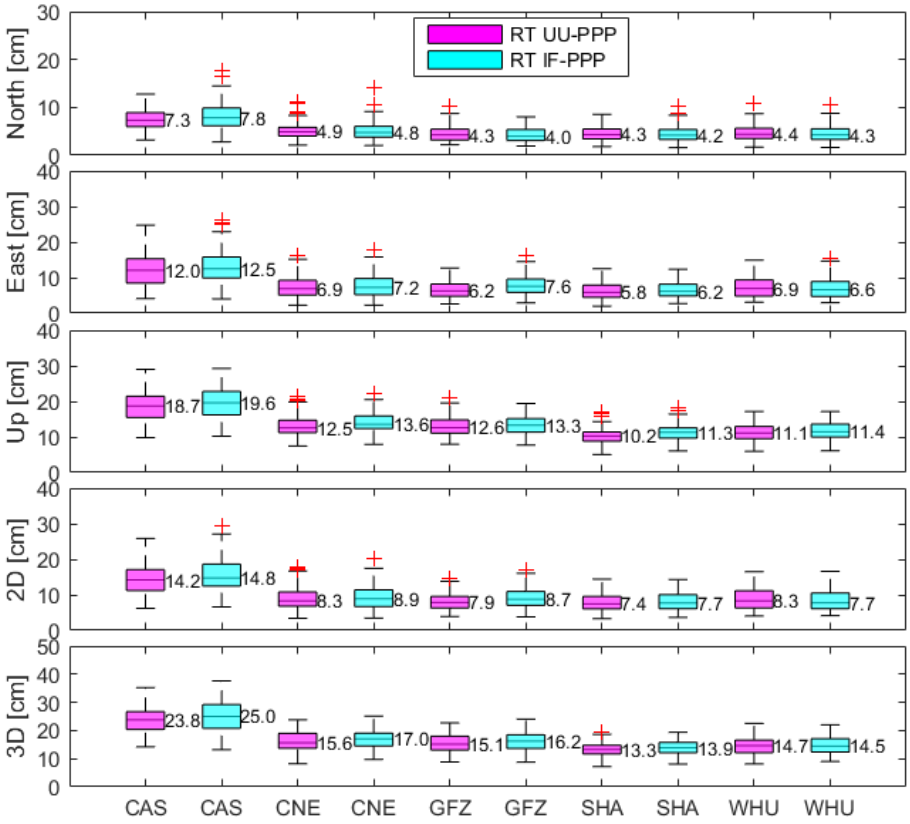

Figure 10. Distribution of RMS positioning accuracy for BDS-2 and BDS-3 joint RT UU-PPP and RT IF-PPP in kinematic mode (20 MGEX stations, DoY 305–316, 2022).

Table 6. Improvement rates of median RMS positioning accuracy for RT UU-PPP compared to RT IF-PPP in kinematic mode (unit: %).

Component	CAS	CNE	GFZ	SHA	WHU
2D	4.1	6.7	9.2	3.9	−7.8
Up	4.6	8.1	5.3	9.7	2.6
3D	4.8	8.2	6.8	4.3	−1.4

5. Conclusions

Compared to the traditional RT IF-PPP, RT UU-PPP has advantages such as lower observation noise and the ability to obtain ionospheric information. Since RTSs have the ability to provide RT-VTEC products, enhanced RT UU-PPP based on the RT-VTEC constraints can be achieved. In this contribution, the quality of RTS orbits and clocks from five ACs was analyzed at first. Then, the global positioning performance of the enhanced BDS-2 and BDS-3 joint RT UU-PPP was investigated.

In RTS orbit quality assessment, the radial orbit accuracy of GFZ, SHAO, and WHU for MEO satellites is at the same level and can be better than 5 cm, while for CAS and CNES, the corresponding accuracy exceeds 7 cm. As for the along-track and cross-track orbit errors, their accuracy for MEO satellites can be better than 14 and 10 cm, respectively. No matter what direction for orbit error, the accuracy of IGSO satellites is lower than that of MEO satellites. In the analysis of RTS clock errors, CAS has the worst clock accuracy in all ACs, and its STD reaches 0.46 ns for MEO satellites. The corresponding accuracy is only 0.2–0.27 ns for other ACs. There is not much difference in IGSO clock accuracy among all ACs, with an STD of 0.4 ns. Compared to previous research from 2021, both the orbit and clock accuracies of BDS RTS products have been improved at the end of 2022, especially for IGSO satellites.

In terms of BDS-2 and BDS-3 joint RT PPP in static mode, the convergence time of RT UU-PPP based on the CNES RT-VTEC constraints is commonly larger than that of RT IF-PPP, which may be caused by the limited accuracy of RTS VTEC products. Due to the lowest clock quality of CAS for MEO satellites, the convergence times of CAS-drive static RT PPP are the longest in all ACs and more than 30 min. Only for static RT UU-PPP, the convergence time of CNES, GFZ, and WHU is at the first level and can be better than 25 min in the horizontal component and 20 min in the vertical component. After convergence, the static positioning accuracy of RT UU-PPP can be improved in both the horizontal and vertical components compared to the RT IF-PPP, and the maximum improvement rate of 3D accuracy is 8.7% in SHAO solutions. The optimal horizontal and vertical positioning accuracies of static RT UU-PPP have the ability to achieve 3.5 and 7.0 cm, respectively, in CNES solutions.

Different from static RT PPP, due to the poor convergence performance of kinematic RT PPP, with the adoption of CNES RT-VTEC constraints, the convergence time of RT UU-PPP can be slightly improved in both the horizontal and vertical components compared to RT IF-PPP. Especially for CAS solutions, their horizontal and vertical convergence time can even be improved by 31.7% and 22.9%, respectively. The kinematic convergence time of GFZ and SHAO is at the first level, with about 55 min in the horizontal component and 60 min in the vertical component. Compared to kinematic RT IF-PPP, the positioning accuracy of RT UU-PPP can be slightly improved in both the horizontal and vertical components, and the maximum improvement rate of 3D accuracy is 8.2% in CNES solutions. For most ACs, the horizontal and vertical positioning accuracy of kinematic RT PPP can be better than 8 and 13 cm, respectively. With the continuous improvement of RTS products for BDS satellites, the vertical positioning accuracy of BDS RT PPP is also expected to achieve the cm level in the future.

Author Contributions: Conceptualization, A.W.; methodology, A.W. and Y.Z.; software, A.W. and Y.Z.; validation, A.W., T.L., M.G. and Q.L.; formal analysis, A.W. and Y.Z.; data curation, T.L., M.G. and Q.L.; writing—original draft preparation, A.W.; writing—review and editing, A.W., Y.Z. and H.W.; supervision, J.C.; funding acquisition, A.W., J.C. and H.W. All authors have read and agreed to the published version of the manuscript.

Funding: This research was funded by the National Natural Science Foundation of China (No. 42304023; No. 42274044), the Fundamental Research Funds for the Central Universities (No. 2022XJDC05), China Postdoctoral Science Foundation (No. 2022M723404), the Program of Shanghai Academic/Technology Research Leader (No. 20XD1404500), and China University of Mining and Technology-Beijing Innovation Training Program for College Students (No. 202302043).

Data Availability Statement: The datasets analyzed in this study are managed by IGS, and data will be made available on request.

Acknowledgments: The authors would like to thank the CAS, CNES, GFZ, SHAO, and WHU for the provision of real-time satellite orbit, clock, VTEC, and code bias products. We also sincerely thank the IGS for the provision of final precise orbit, clock, and MGEX observations.

Conflicts of Interest: The authors declare no conflicts of interest.

References

1. Ge, Y.; Chen, S.; Wu, T.; Fan, C.; Qin, W.; Zhou, F.; Yang, X. An analysis of BDS-3 real-time PPP: Time transfer, positioning, and tropospheric delay retrieval. *Measurement* **2021**, *172*, 108871. [CrossRef]
2. Liu, T.; Zhang, B.; Yuan, Y.; Li, M. Real-Time Precise Point Positioning (RTPPP) with raw observations and its application in real-time regional ionospheric VTEC modeling. *J. Geod.* **2018**, *92*, 1267–1283. [CrossRef]
3. Wang, D.; Huang, G.; Du, Y.; Zhang, Q.; Bai, Z.; Tian, J. Stability analysis of reference station and compensation for monitoring stations in GNSS landslide monitoring. *Satell. Navig.* **2023**, *4*, 29. [CrossRef]
4. Kouba, J.; Héroux, P. Precise point positioning using IGS orbit and clock products. *GPS Solut.* **2001**, *5*, 12–28. [CrossRef]
5. Chen, J.; Li, H.; Wu, B.; Zhang, Y.; Wang, J.; Hu, C. Performance of real-time precise point positioning. *Mar. Geod.* **2013**, *36*, 98–108. [CrossRef]
6. Elsobeiey, M.; Al-Harbi, S. Performance of real-time precise point positioning using IGS real-time service. *GPS Solut.* **2016**, *20*, 565–571. [CrossRef]
7. Hadas, T.; Bosy, J. IGS RTS precise orbits and clocks verification and quality degradation over time. *GPS Solut.* **2015**, *19*, 93–105. [CrossRef]
8. Li, B.; Ge, H.; Bu, Y.; Zheng, Y.; Yuan, L. Comprehensive assessment of real-time precise products from IGS analysis centers. *Satell. Navig.* **2022**, *3*, 12. [CrossRef]
9. Yu, C.; Zhang, Y.; Chen, J.; Chen, Q.; Xu, K.; Wang, B. Performance Assessment of Multi-GNSS Real-Time Products from Various Analysis Centers. *Remote Sens.* **2023**, *15*, 140. [CrossRef]
10. CSNO. *Development of the BeiDou Navigation Satellite System (Version 4.0)*; CSNO: Sacramento, CA, USA, 2019.
11. Liu, P.; Ling, K.; Qin, H.; Liu, T. Performance analysis of real-time precise point positioning with GPS and BDS state space representation. *Measurement* **2023**, *215*, 112880. [CrossRef]
12. Liu, T.; Yuan, Y.; Zhang, B.; Wang, N.; Tan, B.; Chen, Y. Multi-GNSS precise point positioning (MGPPP) using raw observations. *J. Geod.* **2017**, *91*, 253–268. [CrossRef]
13. Li, X.; Han, X.; Li, X.; Liu, G.; Feng, G.; Wang, B.; Zheng, H. GREAT-UPD: An open-source software for uncalibrated phase delay estimation based on multi-GNSS and multi-frequency observations. *GPS Solut.* **2021**, *25*, 66. [CrossRef]
14. Tu, R.; Zhang, P.; Zhang, R.; Liu, J.; Lu, X. Modeling and performance analysis of precise time transfer based on BDS triple-frequency un-combined observations. *J. Geod.* **2019**, *93*, 837–847. [CrossRef]
15. Wang, A.; Zhang, Y.; Chen, J.; Wang, H. Improving the (re-)convergence of multi-GNSS real-time precise point positioning through regional between-satellite single-differenced ionospheric augmentation. *GPS Solut.* **2022**, *26*, 39. [CrossRef]
16. Wang, A.; Chen, J.; Zhang, Y.; Meng, L.; Wang, B.; Wang, J. Evaluating the impact of CNES real-time ionospheric products on multi-GNSS single-frequency positioning using the IGS real-time service. *Adv. Space Res.* **2020**, *66*, 2516–2527. [CrossRef]
17. Liu, Y.; Yang, C.; Zhang, M. Comprehensive analyses of PPP-B2b performance in China and surrounding areas. *Remote Sens.* **2022**, *14*, 643. [CrossRef]
18. Wang, A.; Zhang, Y.; Chen, J.; Wang, H.; Yuan, D.; Jiang, J.; Zhang, Z. Investigating the contribution of BDS-3 observations to multi-GNSS single-frequency precise point positioning with different ionospheric models. *Adv. Space Res.* **2024**, *73*, 553–570. [CrossRef]
19. Xu, Y.; Yang, Y.; Li, J. Performance evaluation of BDS-3 PPP-B2b precise point positioning service. *GPS Solut.* **2021**, *25*, 142. [CrossRef]
20. Zhou, F.; Dong, D.; Li, P.; Li, X.; Schuh, H. Influence of stochastic modeling for inter-system biases on multi-GNSS undifferenced and uncombined precise point positioning. *GPS Solut.* **2019**, *23*, 59. [CrossRef]
21. Jiao, G.; Song, S.; Jiao, W. Improving BDS-2 and BDS-3 joint precise point positioning with time delay bias estimation. *Measur. Sci. Technol.* **2020**, *31*, 025001. [CrossRef]
22. Su, K. BDS pseudorange biases handling: Simultaneous estimation, daily magnitude and analytical comparison of the BDS PPP models. *Adv. Space Res.* **2023**, *71*, 4681–4690. [CrossRef]
23. Zhang, Y.; Kubo, N.; Chen, J.; Wang, A. Calibration and analysis of BDS receiver-dependent code biases. *J. Geod.* **2021**, *95*, 43. [CrossRef]
24. Zhang, Y.; Chen, J.; Gong, X.; Chen, Q. The update of BDS-2 TGD and its impact on positioning. *Adv. Space Res.* **2020**, *65*, 2645–2661. [CrossRef]

25. Chen, H.; Niu, F.; Su, X.; Geng, T.; Liu, Z.; Li, Q. Initial Results of Modeling and Improvement of BDS-2/GPS Broadcast Ephemeris Satellite Orbit Based on BP and PSO-BP Neural Networks. *Remote Sens.* **2021**, *13*, 4801. [CrossRef]
26. Li, B.; Zang, N.; Ge, H.; Shen, Y. Single-frequency PPP models: Analytical and numerical comparison. *J. Geod.* **2019**, *93*, 2499–2514. [CrossRef]